REPORT DOCUMENTATION PAGE

Form Approved OMB NO. 0704-0188

1. REPORT DATE (DD-MM-YYYY)	2. REPORT TYPE	3. DATES COVERED (From - To)
	New Reprint	-

4. TITLE AND SUBTITLE

Sensing of DNA by graphene-on-silicon FET structures at DC and 101GHz

5a. CONTRACT NUMBER
W911NF-09-1-0218

5b. GRANT NUMBER

5c. PROGRAM ELEMENT NUMBER
611102

6. AUTHORS

E.R. Brown, W.-D. Zhang, L. Viveros, D. Neff, N.S. Green, M.L. Norton, P.H.Q. Pham, P.J. Burke

5d. PROJECT NUMBER

5e. TASK NUMBER

5f. WORK UNIT NUMBER

7. PERFORMING ORGANIZATION NAMES AND ADDRESSES

Marshall University Research Corporation
Marshall University Research Corporation
401 11th Street
Huntington, WV 25701 -

8. PERFORMING ORGANIZATION REPORT NUMBER

9. SPONSORING/MONITORING AGENCY NAME(S) AND ADDRESS (ES)

U.S. Army Research Office
P.O. Box 12211
Research Triangle Park, NC 27709-2211

10. SPONSOR/MONITOR'S ACRONYM(S)
ARO

11. SPONSOR/MONITOR'S REPORT NUMBER(S)
55114-EL.12

12. DISTRIBUTION AVAILIBILITY STATEMENT

Approved for public release; distribution is unlimited.

13. SUPPLEMENTARY NOTES

The views, opinions and/or findings contained in this report are those of the author(s) and should not contrued as an official Department of the Army position, policy or decision, unless so designated by other documentation.

14. ABSTRACT

A graphene–silicon field-effect transistor (GFET) structure is demonstrated as a detector of single-stranded 13-mer DNA simultaneously at DC and 101 GHz at three different molarities: 0.01, 1.0 and 100 nM. The mechanism for detection at DC is the DNA-induced change in lateral sheet conductance, whereas at 101 GHz it is the change in RF sheet conductance and the resulting effect on the perpendicular beam transmittance through the GFET acting as an optical etalon. For example, after application and drying of the DNA on a GFET film biased to a DC sheet conductance of 2.22 mS, the 1.0 nM solution is

15. SUBJECT TERMS

Graphene, DNA, THz, DC, Detection

16. SECURITY CLASSIFICATION OF:			17. LIMITATION OF ABSTRACT	15. NUMBER OF PAGES	19a. NAME OF RESPONSIBLE PERSON
a. REPORT	b. ABSTRACT	c. THIS PAGE			Michael Norton
UU	UU	UU	UU		19b. TELEPHONE NUMBER 304-696-6627

Standard Form 298 (Rev 8/98)
Prescribed by ANSI Std. Z39.18

Report Title

Sensing of DNA by graphene-on-silicon FET structures at DC and 101GHz

ABSTRACT

A graphene–silicon field-effect transistor (GFET) structure is demonstrated as a detector of single-stranded 13-mer DNA simultaneously at DC and 101 GHz at three different molarities: 0.01, 1.0 and 100 nM. The mechanism for detection at DC is the DNA-induced change in lateral sheet conductance, whereas at 101 GHz it is the change in RF sheet conductance and the resulting effect on the perpendicular beam transmittance through the GFET acting as an optical etalon. For example, after application and drying of the DNA on a GFET film biased to a DC sheet conductance of 2.22 mS, the 1.0 nM solution is found to reduce this by 1.24 mS with a post-detection signal-to-noise ratio of 43 dB, and to increase the transmitted 101-GHz signal from 0.828 to 0.907 mV (arbitrary units) with a post-detection signal-to-noise ratio of 36 dB. The increase in transmittance is consistent with a drop of the 101-GHz sheet conductance, but not as much drop as the DC value. Excellent sensitivity is also achieved with the 0.01-nm solution, yielding a DC SNR of 41 dB and a 101-GHz SNR of 23 dB.

REPORT DOCUMENTATION PAGE (SF298)
(Continuation Sheet)

Continuation for Block 13

ARO Report Number 55114.12-EL
Sensing of DNA by graphene-on-silicon FET str...

Block 13: Supplementary Note

Approved for public release; distribution is unlimited.

Sensing and Bio-Sensing Research 5 (2015) 19–23

Contents lists available at ScienceDirect

Sensing and Bio-Sensing Research

journal homepage: www.elsevier.com/locate/sbsr

Sensing of DNA by graphene-on-silicon FET structures at DC and 101 GHz

E.R. Brown [a,1], W.-D. Zhang [a,*], L. Viveros [a], D. Neff [b], N.S. Green [b], M.L. Norton [b], P.H.Q. Pham [c], P.J. Burke [c]

[a] Depts. of Physics and Electrical Engineering, Wright State University, Dayton, OH 45435, USA
[b] Department of Chemistry, Marshall University, Huntington, WV 25755, USA
[c] Department of Electrical and Computer Engineering, UC, Irvine, CA 92697, USA

ARTICLE INFO

Keywords:
Graphene
DNA
THz
DC
Detection

ABSTRACT

A graphene–silicon field-effect transistor (GFET) structure is demonstrated as a detector of single-stranded 13-mer DNA simultaneously at DC and 101 GHz at three different molarities: 0.01, 1.0 and 100 nM. The mechanism for detection at DC is the DNA-induced change in lateral sheet conductance, whereas at 101 GHz it is the change in RF sheet conductance and the resulting effect on the perpendicular beam transmittance through the GFET acting as an optical etalon. For example, after application and drying of the DNA on a GFET film biased to a DC sheet conductance of 2.22 mS, the 1.0 nM solution is found to reduce this by 1.24 mS with a post-detection signal-to-noise ratio of 43 dB, and to increase the transmitted 101-GHz signal from 0.828 to 0.907 mV (arbitrary units) with a post-detection signal-to-noise ratio of 36 dB. The increase in transmittance is consistent with a drop of the 101-GHz sheet conductance, but not as much drop as the DC value. Excellent sensitivity is also achieved with the 0.01-nm solution, yielding a DC SNR of 41 dB and a 101-GHz SNR of 23 dB.

1. Introduction

Graphene continues to attract attention for its application to biosensing, particularly the detection of trace concentrations of macromolecules such as nucleic acids and proteins [1]. This is justified largely by the strong covalent sp^2-hybridized bonding behavior that graphene displays [2]. However, like so many other biosensors, graphene-based detectors present significant challenges in selectivity not only between macromolecular types but between different forms of the same type, such as different base sequences of DNA or RNA [3]. This is because the sp^2 bonding is sensitive to the primary molecular structure, but not so much to the secondary or tertiary structure [4]. One possible method of discriminating macromolecules based on higher-order structure is through their $\pi-\pi$ stacking [5] and high-frequency dielectric behavior [6,7]. Theoretical and experimental studies have long shown the presence of unique dielectric dispersion and low-lying vibrational resonance in macromolecules, especially the nucleic acids [8]. The research presented here is relevant to the longstanding proposal that biosensor selectivity between macromolecules may ultimately be attained by virtue of these unique signatures, especially at millimeter-wave and THz frequencies [9–11].

In a recent publication we demonstrated the utility of a graphene-oxide–silicon resonator structure in determining the THz complex conductance of graphene [12]. A cross-sectional view of the structure is shown in Fig. 1(a), and the fabrication method entails transfer of a low-pressure chemical vapor deposition (LPCVD)-prepared, monolayer graphene film oxide-pre-coated, high-resistivity silicon substrate [13]. Then source (S) and drain (D) contacts are deposited directly on the graphene, and a gate (G) contact on the opposite side of the silicon to create a graphene-channel field-effect transistor (GFET). Although having relatively low transconductance by Si-MOS standards, this GFET is quite useful for studying the transport physics of graphene, especially in comparing the high-frequency (THz) behavior to the low-frequency (DC) behavior. For example, from interference effects displayed in the transmission of normally incident radiation, it was found that the real parts of the dc and THz sheet conductances are quite comparable, consistent with the Drude model [14]. Here, we utilize the same GFET but for biomolecular sensing via the exposed topside graphene film with the electrodes used for tuning and calibration of the sheet conductance. The same type of graphene film has already been demonstrated for chemical detection but on a PDMS substrate rather than the Si used here [15]. The effect of the biomolecules on the high frequency sheet conductance

* Corresponding author. Tel.: +1 (937)775 4903.
E-mail addresses: elliott.brown@wright.edu (E.R. Brown), wzzhang@fastmail.fm (W.-D. Zhang).
[1] Tel.: +1 (937)775 4903.

http://dx.doi.org/10.1016/j.sbsr.2015.05.002
2214-1804/

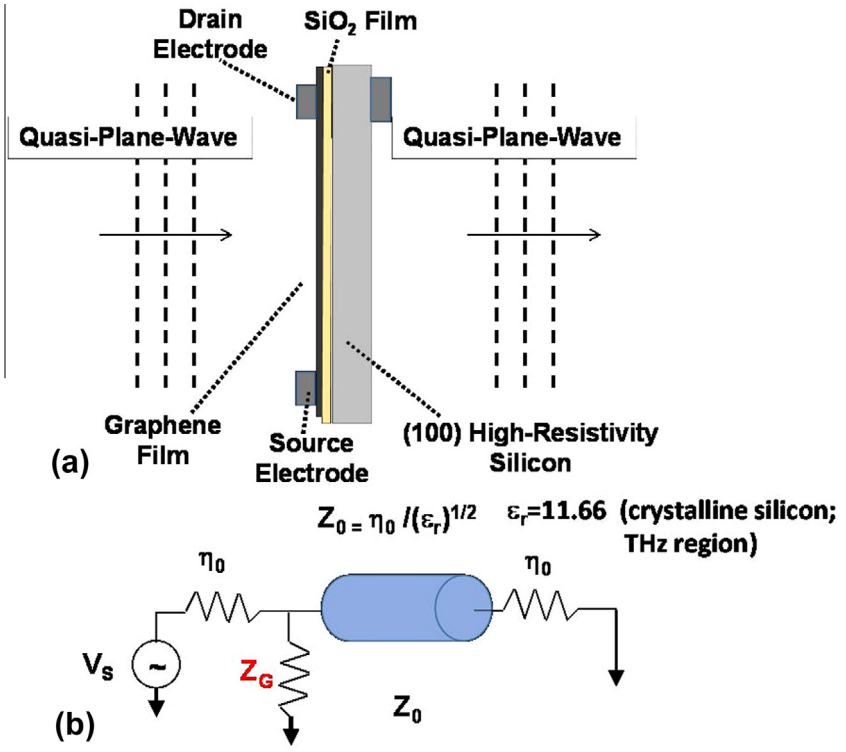

Fig. 1. (a) GFET structure, and (b) transmission-line model for calculation of transmittance.

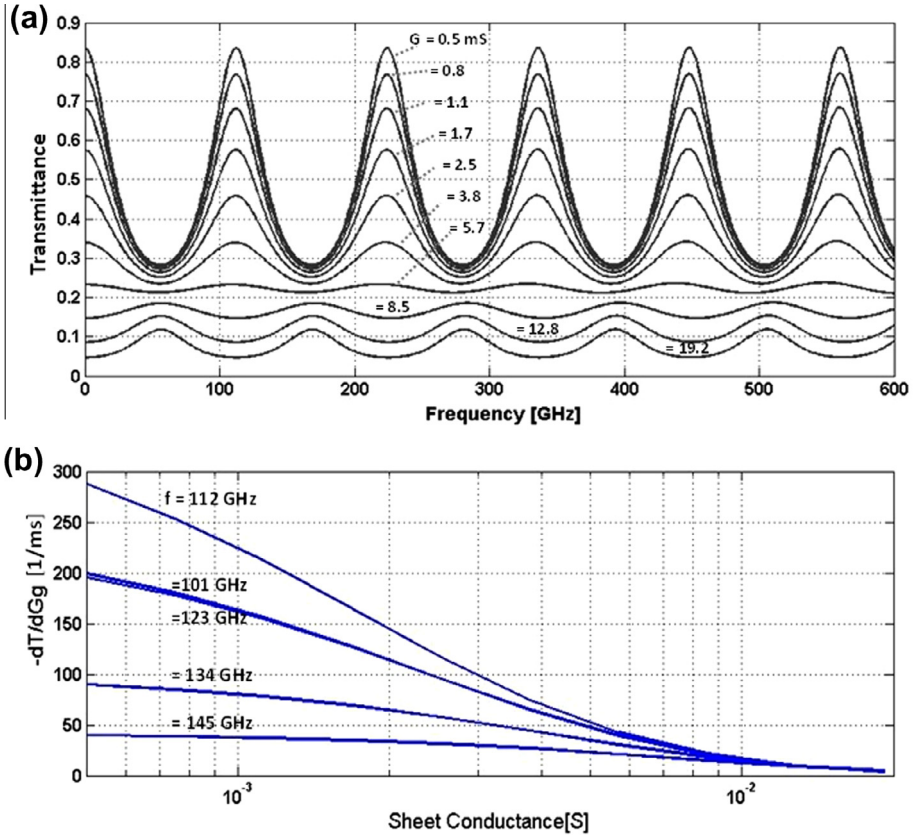

Fig. 2. Transmittance and its sensitivity factor as a function of graphene sheet conductance.

is estimated via the transmittance T of radiation propagating perpendicular to the graphene, as shown in Fig. 1(a). Assuming quasi-plane-wave radiation, we can model T with the transmission line model in Fig. 1(b) in which graphene is simply a shunt, lumped impedance Z_G. The length of the transmission line L is equal to the thickness of the high-resistivity silicon substrate, and its characteristic impedance Z_0 is equal to $\eta_0/n = 110\,\Omega$, where $n = \varepsilon_r^{1/2} = 3.415$ and $\varepsilon_r = 11.66$: the relative dielectric constant of the Si in the 100–1000 GHz range [16]. Circuit analysis then predicts T as the ratio between the power delivered to the free space load (lumped element η_0) and the available power from the source on the incident side.

Fig. 2(a) shows the predicted T as a function of frequency and parameterized by sheet impedance assuming the imaginary part is negligible so that $Z_G \approx 1/G_G$. Our previous results showed that this approximation is quite valid at ~100 GHz but becomes less accurate with increasing frequency [12]. The range of parametrized sheet conductance G_G is 0.5–19.2 mS, corresponding to $8G_0$—$316G_0$, where $G_0 = \pi e^2/2h$ is the optical (interband) conductance in graphene [17]. The graphene tested in this work typically displays dc conductance between 1.2 and 2.2 mS (20–35G_0) consistent with the intraband conductivity being much higher than the interband in single-layer graphene. For each G in Fig. 2, T displays the oscillatory Airy-function behavior characteristic of all parallel-plate etalons (and Fabry–Perot resonators) with peak-to-peak separation $\Delta f = c/2nL = 112$ GHz for L=392 μm. The peaks do not quite reach unity transmission since the etalon is optically unbalanced, the graphene side having a higher sheet conductance than the opposite air-interface side.

Most important for our bio-detection experiments is the variation of the transmittance with sheet conductance-a quantity we call the sensitivity factor and estimate as the first derivative $\partial T/\partial G_G|_f$. By visual inspection of Fig. 2 we expect the sensitivity factor to be much greater near the peaks of T than near the valleys. This is quantified graphically in Fig. 2(b) where we plot the computed dT/dG_G vs G_G and parametrized by frequency around the first-nonzero-frequency peak (fundamental resonance) in 2(a) centered at 112 GHz. For $G_G = 1.0$ mS, we see $\partial T/\partial G_G|_f$ drops by 5× between 112 and 145 GHz. This behavior is consistent with the fact that the peaks in T are points of perfect constructive interference of successive internal partial waves, so are most sensitive to small changes in the reflectivity of the graphene interface.

2. Experiments

Fig. 2(b) guided our design of the experimental sensor apparatus shown schematically in Fig. 3. It consists of a waveguide-mounted Gunn-oscillator operating at a fixed frequency of 101 GHz just 11 GHz below the fundamental resonance of the graphene–silicon etalon. It is square-wave amplitude modulated with a power-MOSFET circuit, radiated horizontally through a pyramidal horn antenna that feeds an off-axis paraboloid which directs and focuses the beam downward. The focused beam is mode-matched to a second feedhorn that collects the radiation into a Schottky-rectifier receiver. The GFET structure is then located in the beam path just above the receive feedhorn where the spot size is approximately 5 mm. The output signal from the Schottky rectifier is fed to a 1000×-gain low-noise voltage amplifier, and then demodulated with a lock-in amplifier synchronized to the square wave. A waveguide attenuator between the Gunn oscillator and the feedhorn allows the received signal to be increased to the maximum possible output signal-to-noise ratio (SNR) before the onset of compression and other nonlinearity. Typically, this background SNR was ~60 dB.

3. Results and discussions

The GFET structure was operated with the backgate bias of $V_{GS} = +25$ V from a low-noise power supply, and a drain-source constant-voltage bias of $V_{DS} = +0.1$ V from a Keithley 2400 source meter. This backgate bias was chosen because of its proximity to the Dirac-point bias of ~30 V, which was attainable but only with a large degree of fluctuation in the drain-source current. The 25 V backgate bias creates a significant background electron sheet concentration in the graphene, and the V_{DS} is just high enough to allow accurate measurement of the sheet conductance without excessive drift and 1/f noise. Because the graphene geometry between the S and D electrodes is approximately square (area ≈ 1 cm^2), the absolute DC sheet conductance is $G_{DC} \approx I_{DS}/V_{DS}$. For the specific GFET tested we measured an I_{DS} of 0.2132 mA, or sheet conductance of 2.132 mS. The corresponding background 101-GHz transmittance signal was $X_B = 0.8527$ V where the last digit is significant given the high SNR.

To validate the measurement technique and assess its accuracy, we used the backgate to induce a known-change in graphene DC

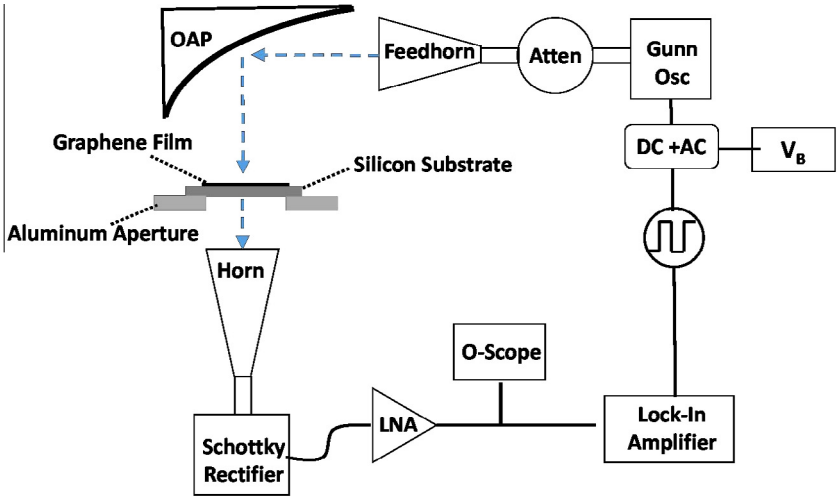

Fig. 3. The 101 GHz GFET sensing setup.

sheet conductance and compare this with the derived change of the 101-GHz quantity. We applied backgate voltages of $V_{HI} = 30$ V and $V_{LO} = 20$ V to straddle the nominal +25 V and allow for mean-value estimation. The DC current values at the two gated voltages were 0.2017 and 0.2255 mA, respectively, corresponding to $\Delta G_{DC} = \Delta I/0.1 = -0.238$ mS. The lock-in signals for the same backgate voltages were $X_{HI} = 0.8661$ and $X_{LO} = 0.8412$ corresponding to a transmittance difference of $T_{HI} - T_{LO} \approx (X_{HI} - X_{LO})/X_B = 0.0292$. Division by $\partial T/\partial G_G \approx -0.11\ \mathrm{mS}^{-1}$ then yields $\Delta G_{RF} \approx -0.265$ mS in good agreement with ΔG_{DC}.

The biodetection protocol was to apply 13-mer single-stranded DNA solutions of three different molarities (0.01, 1.0, and 100 nM) sequential at 900-s intervals, starting with the 0.01 nM solution. A drop of each was placed directly on the graphene with a syringe, allowed to settle for 300 s, and then blown dry with an oil-free air gun. The Keithley-2400 DC current was recorded simultaneous with the THz transmitted signal via the output from the lock-in amplifier. The experimental results for DC current are shown in Fig. 4(a) where we see an initial value of 222 μA between ≈600 and 900 s, corresponding to a sheet conductance of 2.22 mS. Then a large fall in DC current occurs with the application of all three drops, and a lesser fall upon blow drying 300 s later. Both effects are most pronounced with the 0.01 nM solution and become progressively weaker with the other two. The 1.0 and 100 nM drops have a significant effect in their aqueous form but little further change occurs upon drying. In all cases, however, at constant bias voltage the DNA decreases the DC sheet conductance of the graphene.

Similarly, the transmitted THz signal plotted in Fig. 4(b) shows a large and precipitous decrease upon application of each drop of DNA solution. But unlike the DC current, the THz signal recovers to its previous level and goes slightly higher upon drying. The decrease and recovery can be explained by the strong absorption coefficient of $\sim 100\ \mathrm{cm}^{-1}$ for liquid water at 101-GHz. Although each drop is ~1 mm thick, they don't fill the entire beam footprint in Fig. 3 so the net attenuation caused by the liquid water is only ~3 dB. From Fig. 2, the increased post-dry transmission level compared to initial level suggests that the 101-GHz sheet conductance, like the DC conductance, is decreasing with each drop.

To quantify and compare the effects of the DNA on the DC and 101-GHz signals, we define and calculate relative sheet- conductance changes, ΔG_{DC} and ΔG_{RF}. The former is defined according to Fig. 4(a) as $\Delta G_{DC} = (I_N - I_0)/0.1$ V, where the I_N ($N = 1$, 2, and 3) are the plateau (time-averaged) current levels after thorough drying of the 0.01, 1.0, and 100 nM drops, respectively. The latter is defined by $\Delta G_{RF} = [(X_N - X_0)/X_0]/[\partial T/\partial G_G]$ where the X_N ($N = 1$, 2, and 3) are the corresponding plateau transmittance signals, and again $\partial T/\partial G_G \approx -0.11\ \mathrm{mS}^{-1}$. A plot of these quantities vs molarity is displayed in Fig. 5 showing a monotonic increase in absolute value but a relatively small change in slope vs molarity, especially for the ΔG_{DC} which changes less than 40% over the entire range. Interestingly, the ΔG_{RF} is always smaller in magnitude, especially for 0.01 nM where it is approximately 5-times lower. The reason for this is not yet understood.

Finally, we can obtain a metric for the sensitivity of both methods by calculation of the post-detection signal-to-noise ratio (SNR). For the DC method the SNR is just $\Delta I_{DC}/I_{rms} = |I_N - I_0|/I_{rms}$ where I_{rms} is the rms fluctuation dominated by a fast (white noise) component from the current source (Keithley 2400), and a slow (drift) component from the graphene. The noise was observed over a 600 s time span with the graphene kept dry, and yielded $I_{rms} \approx 8.5 \times 10^{-7}$ A. Thus, for the 1.0 nM case with $\Delta I_{DC} \approx 0.124$ mA, we get an SNR of 145 [43.2 dB power SNR]. And for the 0.01 nM case with $\Delta I_{DC} \approx 0.010$ mA, the DC-SNR is 117 [41 dB]. The DC SNR

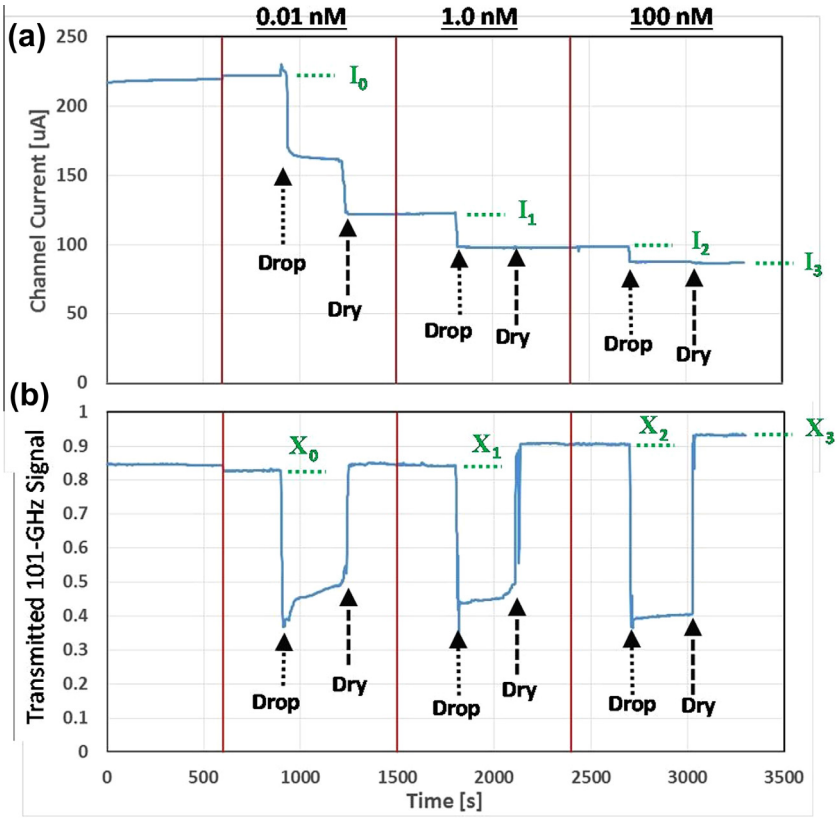

Fig. 4. The effects of DNA on DC and 101-GHz signals.

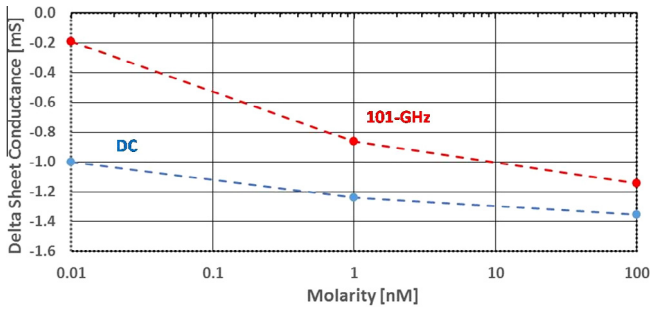

Fig. 5. The varivation of graphene sheet conductance vs molarity at DC and 101 GHz.

drops only 2 dB for the two-order lower molarity, which bodes well for detecting even smaller concentrations but the nonlinearity precludes an extrapolation in that direction.

For the 101-GHz method the SNR is $\Delta X_{RF}/X_{rms} = |X_N - X_0|/X_{rms}$ where X_{rms} is the lock-in output noise which was attributable primarily to white-noise from the Schottky rectifier and the low noise amplifier (LNA). Observed over the same 600 s time window, and for the given modulation frequency (1 kHz) and integration time (0.3 ms), we measured $X_{rms} = 1.22$ mV. Thus for the 1.0 nM case where $|X_1 - X_0| = 0.079$ mV, the SNR = 64.6 [36.2 dB power SNR]. And for the 0.01 nM case where $|X_1 - X_0| = 0.017$ mV, the SNR = 14.0 [23 dB]. The 101-GHz SNR drops 13 dB for the two-order lower molarity, more than the DC drop, but still nonlinear. Interestingly, the ~7 dB lower SNR for the 101-GHz signal is very close to the degree of sub-optimal performance according to Fig. 2(b). If the operating frequency was 112 instead of 101 GHz, and the DC sheet conductance was 1.0 mS instead of the 2.1 mS displayed by the present device, then the sensitivity factor would be ≈2× higher and the post-detection SNR ≈ 6 dB higher than the result reported here. In principle, this lower sheet conductance could be obtained by increasing the backgate voltage, but even 50 V only reduced it to about 1.5 mS and the drain-source current was noticeably unstable at this point. Alternately, one should get ~3 dB improvement in SNR by starting with a thicker Si substrate (435 μm) for which the first non-zero resonance in Fig. 2(a) would occur at 101 instead of 112 GHz.

4. Conclusion

In conclusion, we have presented the first known detection of DNA by single-layer graphene simultaneously at DC and a millimeter-wave frequency, specifically 101 GHz. Although the DC detection is more sensitive in terms of SNR in the tested GFET structure, there is room for improvement in the mm-wave performance through optimization of the experimental parameters. The mm-wave detection opens up the exciting possibility of enhancing the selectivity of the GFET towards nucleic acids vs many other possible analytes by further characterization of the frequency-dependence and possible vibrational resonances that nucleic acids are known to display at radio frequencies above ~10 GHz.

This material is based upon work supported by, or in part by, the U.S. Army Research Laboratory and the U.S. Army Research Office under contract number W911NF-11-1-0024.

Conflict of interest

The authors declare that they have no conflict of interest.

References

[1] N.S. Green, M.L. Norton, Interactions of dna with graphene and sensing applications of graphene field-effect transistor devices: a review, Anal. Chim. Acta 853 (2015) 127–142.
[2] S. Manohar, A.R. Mantz, K.E. Bancroft, C.Y. Hui, A. Jagota, D.V. Vezenov, Peeling single-stranded dna from graphite surface to determine oligonucleotide binding energy by force spectroscopy, Nano Lett. 8 (2008) 4365–4372.
[3] X.-C. Dong, Y.-M. Shi, W. Huang, P. Chen, L.-J. Li, Electrical detection of dna hybridization with single-base specificity using transistors based on cvd-grown graphene sheets, Adv. Mater. 22 (2010) 1649–1653.
[4] C.T. Lin, P.T. Loan, T.Y. Chen, K.K. Liu, C.H. Chen, K.H. Wei, label-free electrical detection of dna hybridization on graphene using hall effect measurements: revisiting the sensing mechanism, Adv. Funct. Mater. 23 (2013) 2301–2307.
[5] E. Dubuissona, Z. Yang, K.-P. Loh, Optimizing label-free dna electrical detection on graphene platform, Anal. Chem. 83 (2011) 2452–2460.
[6] J. Lee, J.G. Yook, Recent research trends of radio-frequency biosensors for biomolecular detection, Biosens. Bioelectron. 61 (2014) 448–459.
[7] I. Iramnaaz, Y. Xing, K. Xue, Y. Zhuang, R. Fitch, Graphene based rf/microwave impedance sensinof dna, IEEE Electron. Compon. Tech. Conf. 61 (2011) 1030–1034.
[8] R. Holzel, Dielectric and dielectrophoretic properties of dna, IET Nanobiotechnol. 3 (2009) 28–45.
[9] A. Wittlin, L. Genzel, F. Kremer, D. Häseler, A. Poglitsh, Phys. Rev. A 34 (1986) 493–500.
[10] T.R. Globus, D.L. Woolard, T. Khromova, T.W. Crowe, M. Bykhovskaia, B.L. Gelmont, J. Hesler, A.C. Samuels, J. Biol. Phys. 29 (2003) 89–100.
[11] P. Zhao, B. Woolard, Influence of base-pair interaction on vibrational spectrum of a poly-dg molecule bonded to si substrates, IEEE Sens. J. 8 (2008) 998–1003.
[12] W.-D. Zhang, P.H.Q. Pham, E.R. Brown, P.J. Burke, Ac conductivity parameters of graphene derived from thz etalon transmittance, Nanoscale 6 (2014) 13895–13899.
[13] N. Rouhi, S. Capdevila, D. Jain, K. Zand, Y.-Y. Wang, E.R. Brown, L. Jofre, P. Burke, Thz graphene optics, Nano Res. 5 (2012) 667–678.
[14] L.A. Falkovsky, Optical properties of graphene and iv–vi semiconductors, Phys. Usp. 51 (2008) 887–897.
[15] Y.-Y. Wang, P. Burke, A large-area and contamination-free graphene transistor for liquid-gated sensing applications, Appl. Phys. Lett. 103 (2013) 052103.
[16] P.H. Bolivar, M. Brucherseifer, J.G. Rvivas, R. Gonzalo, I. Ederra, A.L. Reynolds, M. Holker, P. Mgt, Measurement of the dielectric constant and loss tangent of high dielectric-constant materials at terahertz frequencies, IEEE Trans. Microwave Theory Tech. 51 (2003) 1062–1066.
[17] K.-F. Mak, M. Sfeir, Y. Wu, C.-H. Lui, J. Misewich, T. Heinz, Measurement of the optical conductivity of graphene, Phys. Rev. Lett. 101 (2008) 196405.